Journal of Petroleum Science and Engineering 195 (2020) 107442

Contents lists available at ScienceDirect

Journal of Petroleum Science and Engineering

journal homepage: http://www.elsevier.com/locate/petrol

Simulation of solvent treatments for fluid blockage removal in tight formations using coupled three-phase flash and capillary pressure models

Sajjad S. Neshat *, Ryosuke Okuno, Gary A. Pope

The University of Texas, Austin, USA

ARTICLE INFO

Keywords:
Unconventional EOR
Solvent
Shale gas
Solvent.
Capillary pressure
Phase behavior

ABSTRACT

Water and condensate blockage near production wells in unconventional reservoirs can significantly reduce oil and gas production rates. This paper presents a new approach for more accurate modeling of liquid blockage in tight oil and gas reservoirs and investigates the use of solvents for blockage removal. A cubic equation of state is used to model mixtures of solvent, hydrocarbons and water that form up to three phases. The three-phase flash model is coupled with a three-phase capillary pressure model to account for the effect of capillary pressure in confined space. The capillary pressure function includes the impact of several important petrophysical properties such as pore size distribution and wettability. A compositional simulator is used to demonstrate the importance of the new phase behavior model. Single- and multi-cycle processes of methanol, dimethyl ether or CO_2 injection are simulated to remove liquid blockage and increase production rate in tight oil/gas reservoirs. Simulation results show that DME is more efficient than methanol and CO2 for removal of liquid blockage in tight oil/gas reservoirs because DME is miscible with both oil and water under the simulated reservoir conditions.

1. Introduction

Sustainable production from unconventional oil and gas reservoirs has become a priority for the industry as these resources continue to make a significant contribution to the global energy supply. Advanced horizontal drilling and hydraulic fracturing technologies have allowed economic production from tight formations, but rapid decline in production rate in low permeability reservoirs is still a major issue. Most tight formations initially have low water saturation, but during the well completion process, vast quantities of fracturing fluids are injected. Only a fraction of the injected water is recovered and much of it is trapped in small pores of the matrix (Gupta, 2009). The increased water saturation near hydraulic fractures lowers the relative permeability of hydrocarbon phases and impairs production rates (Bertoncello et al., 2014). In gas-condensate reservoirs, the retrograde behavior of hydrocarbon mixtures can accentuate the problem of liquid blockage. When the bottomhole pressure falls below the dew point pressure, condensate drops out and builds up near the wells. The condensate blocks gas flow in the pores and lowers the gas relative permeability (Pope et al., 2000).

The use of solvents to remove liquid blockage and restore well deliverability in conventional reservoirs has been extensively studied both experimentally and numerically (Sayed and Al-Muntasheri, 2016). Methane and CO_2 have a very small solubility in water and cannot remove water blockage whereas light alcohols such as methanol (MeOH) are miscible with water. MeOH has been used to remove liquid blockage and increase production rate (Al-Anazi et al., 2005). Due to the limited solubility of MeOH in oil or condensate (Bang et al., 2010a,b), Ganjdanesh et al. (2016) proposed the use of dimethyl ether (DME) and compared its efficiency in removing water and condensate blockage within hydraulic fractures with light alcohols such as MeOH. They showed that using DME results in higher efficiency since it is miscible with both water and condensate under reservoir conditions. However, they neither investigated liquid blockage and its treatment inside the matrix of tight formations nor included formation heterogeneity.

Tight and shale formations consist of very small pores with wide and complex pore size distributions ranging from 5 to 200 nm (Nelson, 2009). At this scale, the phase behavior of reservoir fluids deviates from the bulk behavior. This deviation is due in part to the effect of high capillary pressure. Several authors have used a single-tube capillary pressure model with a fixed radius to calculate the effect of capillary pressure on two-phase equilibrium (Brusilovsky, 1992; Nojabaei and Johns, 2013; Sanaei et al., 2014; Sherafati and Jessen, 2017; Nichita, 2018). However, capillary pressure also depends on pore size distribution, phase saturations, wettability, in interfacial tension, porosity and

* Corresponding author.
E-mail address: ssneshat@utexas.edu (S.S. Neshat).

https://doi.org/10.1016/j.petrol.2020.107442
Received 22 May 2019; Received in revised form 15 May 2020; Accepted 19 May 2020
Available online 13 June 2020

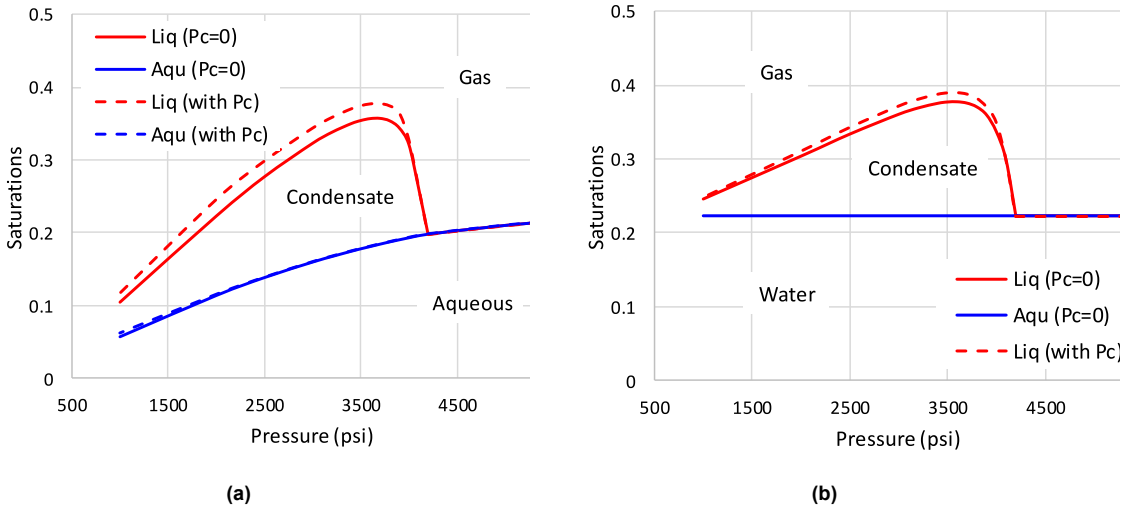

Fig. 1. Phase behavior of Eagle Ford gas-condensate at 210 °F using (a) the new coupled three-phase flash and capillary pressure models and (b) a two-phase flash including oil-gas capillary pressure at constant 22.3% water saturation. Solid and dashed lines show the calculations without and with the effect of capillary pressure.

Table 1
PR EOS parameters for Eagle Ford gas-condensate.

	Mole %	Molecular weight (lb/lb-mol)	Critical pressure (psia)	Critical Temperature (°R)	Parachor	Acentric factor	Volume shift (ft^3/lb-mol)
H_2O	50.00	18.01	3203.72	1165.14	54.0	0.344	0.049
CO_2	1.44	44.01	1069.87	547.89	78.0	0.225	−0.026
C_1	35.42	16.04	673.08	343.26	77.3	0.013	−0.154
C_2	4.48	30.07	708.35	549.77	108.9	0.097	−0.100
C_3	2.49	44.10	617.38	665.82	151.9	0.152	−0.085
C_{4-6}	2.63	65.94	510.61	816.77	218.9	0.230	−0.081
C_{7-14}	3.42	135.54	354.70	1145.04	388.2	0.455	0.148
C_{15+}	0.12	233.10	246.10	1356.30	659.1	0.684	1.084
MeOH	0.00	32.05	1174.21	923.04	80.0	0.559	0.111
DME	0.00	46.07	789.39	720.51	132.7	0.200	0.000

Table 2
PR EOS binary interaction coefficients (BICs) used for Eagle Ford gas-condensate.

	H_2O	CO_2	C_1	C_2	C_3	C_{4-6}	C_{7-14}	C_{15+}	MeOH	DME
H_2O	0									
CO_2	0.095	0								
C_1	0.55	0.1	0							
C_2	0.55	0.13	0	0						
C_3	0.52	0.135	0	0	0					
C_{4-6}	0.52	0.125	0	0	0	0				
C_{7-14}	0.55	0.111	0.024	0.02	0.014	0.005	0			
C_{15+}	0.55	0.082	0.074	0.05	0.03	0.02	0	0		
MeOH	−0.275	0.29	0.29	0.29	0.25	0.20	0.075	0.075	0	
DME	−0.17	0.25	0.25	0.25	0.2	0.15	0.05	0.05	0	0

Table 3
Capillary pressure parameters.

	Eagle Ford	Middle Bakken
k	0.5 μD	5 μD
φ	10%	6%
a_g	0.07	0.07
a_a	0.95	0.95
$a_{o\ (oil\text{-}gas)}$	1.05	1.05
$a_{o\ (oil\text{-}aqu)}$	1.05	1.05
b_g	−9	−3.3
b_a	3.6	1.3
$b_{o\ (oil\text{-}gas)}$	23	8
$b_{o\ (oil\text{-}aqu)}$	−2	−0.74

permeability. Neshat et al. (2018) presented a rigorous solution to the problem of phase behavior in tight formations coupled with three-phase capillary pressure. Using a new criterion for stability analysis and selection of the cubic equation of state (EOS) roots, they found a continuous solution to gas-oil equilibrium in the presence of water over the whole range of pore sizes typically found in unconventional reservoirs. Neshat et al. (2018) included the effect of water on the gas-oil capillary pressure, but they neglected the solubility of water in the hydrocarbon phases. They did not do a three-phase flash calculation with capillary pressure. Using different tight oil and gas-condensate mixtures, they showed that capillary pressure can have a noticeable impact on oil-gas phase behavior especially at low water saturations. Sandoval et al. (2019) used an alternative method to include the effect of pore size

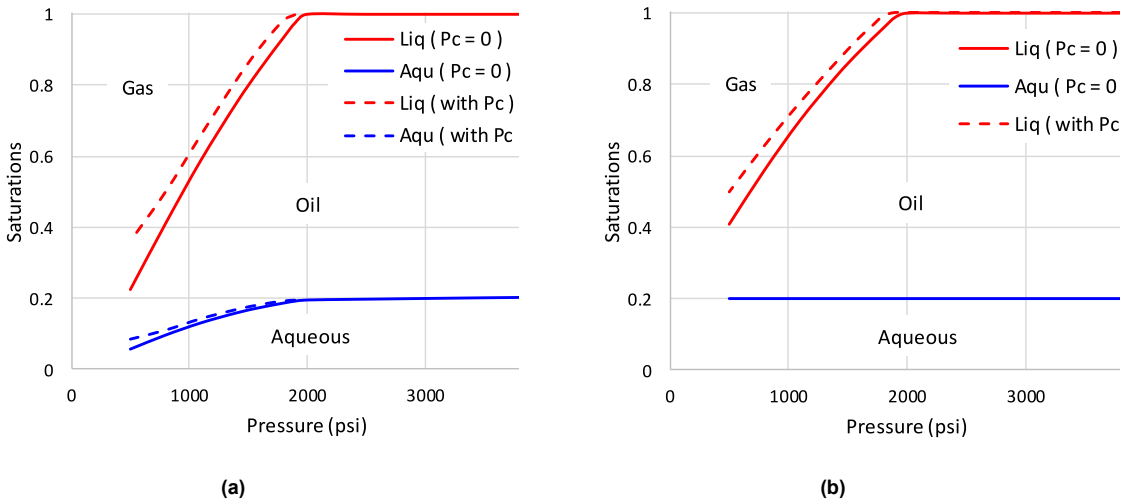

Fig. 2. Phase behavior of Middle Bakken tight oil at 200 °F using (a) the new coupled three-phase flash and capillary pressure models and (b) a two-phase flash considering oil-gas capillary pressure at constant 20% water saturation. Solid and dashed lines show the calculations without and with the effect of capillary pressure.

Table 4
PR EOS parameters for Middle Bakken oil.

	Mole %	Molecular weight (lb/lb-mol)	Critical pressure (psia)	Critical temperature (°R)	Parachor	Acentric factor	Volume shift (ft^3/lb-mol)
H_2O	0.35	18.01	3203.72	1165.14	54.0	0.344	0.049
CO_2	0.01	44.01	1069.86	547.56	78.0	0.225	−0.03
C_1	16.33	16.04	667.19	343.08	77.0	0.008	−0.08
$C_{2\text{-}4}$	14.22	42.82	625.16	653.94	145.2	0.143	−0.1
$C_{5\text{-}7}$	13.02	83.74	496.13	920.81	250.0	0.247	0.02
$C_{8\text{-}9}$	8.43	105.91	454.25	1042.81	306.0	0.286	0.11
C_{10+}	12.96	200.00	317.14	1419.73	686.3	0.687	0.74

Table 5
PR EOS binary interaction coefficients (BICs) used for Middle Bakken oil.

	H_2O	CO_2	C_1	C_2–C_4	C_5–C_7	C_8–C_9	C_{10+}	MeOH	DME
H_2O	0								
CO_2	0.095	0							
C_1	0.55	0.1	0						
C_2–C_4	0.52	0.135	0.008	0					
C_5–C_7	0.55	0.141	0.024	0.0046	0				
C_8–C_9	0.55	0.15	0.032	0.0087	0.001	0			
C_{10+}	0.55	0.15	0.078	0.0384	0.017	.011	0		
MeOH	−0.275	0.29	0.29	0.25	0.2	0.075	0.075	0	
DME	−0.17	0.25	0.25	0.2	0.15	0.05	0.05	–	0

distribution in phase split calculations through J-function.

When solvents mix with reservoir fluids, the phase behavior of the mixture becomes complex and a three-phase flash is required to define the equilibrium condition between aqueous, oil and gas phases. Bang et al. (2010a, 2010b) did extensive experimental studies on the phase behavior of solvents such as MeOH, ethanol (EtOH) and propylene glycol (PG) with mixtures of water and hydrocarbons. They showed that the Peng-Robinson (PR) EOS model with tuned binary interaction coefficients (BICs) and volume shift parameters (VSPs) matched their experimental data. Ganjdanesh et al. (2016) found that a tuned PR EOS model matched experimental DME data (Tallon and Fenton, 2010). More complex mixing rules have been proposed in the literature to improve accuracy (Ratnakar et al., 2017). In tight formations with very small pores, the capillary pressure across highly curved phase interfaces can exceed hundreds of psi and affect the equilibrium state of all three phases. This effect must be accounted for when using solvent enhanced oil recovery (EOR) methods in tight formations is considered.

Several authors have used numerical simulation to include the effect of capillary pressure on phase behavior of hydrocarbon phases during primary production from tight reservoirs (Jiamin and Younis, 2016; Siripatrachai et al., 2017; Sanaei et al., 2014). However, there were limitations in both the petrophysical and thermodynamic models used in these studies. For example, the impact of water on oil-gas capillary pressure was not included in some studies although it is known to be influential (Neshat et al., 2018). The bottomhole pressure in tight formations is typically set much lower than initial reservoir pressure to increase the production rate. The solubility of water in the gas phase can significantly increase at lower pressures (Bang, 2010 a), which affects interfacial tension (IFT) and thus the capillary pressure between the phases.

In this study, coupled three-phase flash and capillary pressure models are presented for simulation of tight oil and gas reservoirs. The capillary pressure between each phase pair is calculated using a three-phase capillary pressure model that integrates the impact of important

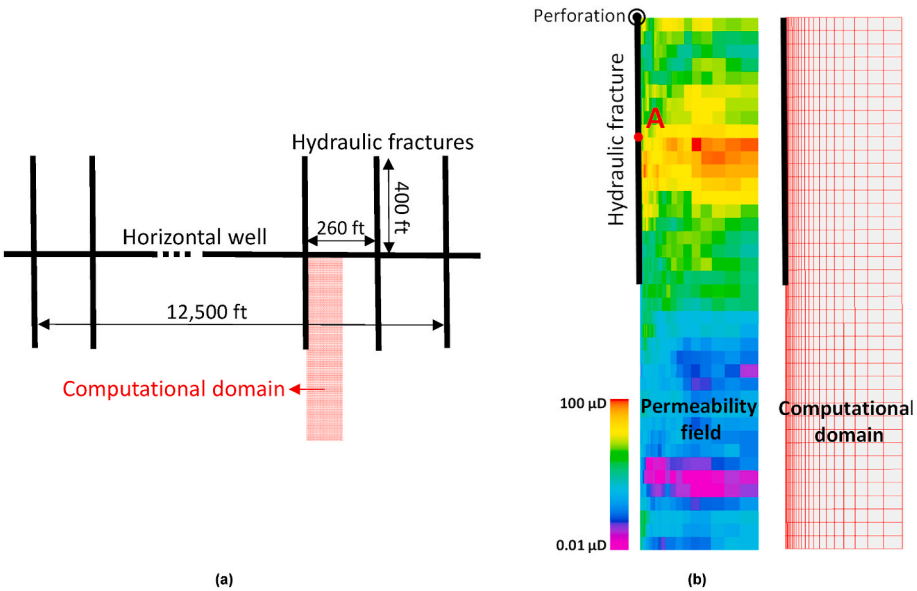

Fig. 3. Configuration of (a) horizontal well and hydraulic fractures and (b) randomly generated heterogeneous permeability field and the computational domain. The well is perforated only at its intersection with the hydraulic fractures.

Table 6
Reservoir properties (Eagle Ford).

Depth	10,000 ft
Reservoir thickness	300 ft
P (initial)	9000 psi
Dew point pressure	4220 psi
Condensate to gas (CGR) ratio	100
Temperature	210 °F
Matrix Porosity	10%
Fracture porosity	30%
Fracture permeability	5 D
DME/MeOH Molecular diff. coef.	0.001 ft^2/Day
Longitudinal dispersivity	30 ft
Tortuosity	150
S_w (initial)	20%
Production well BHP	2500 psi

Table 7
Relative permeability reference values (Eagle Ford). R and T are the universal gas constant and reservoir temperature, respectively.

	k_r^0	S_r	n	Trapping number coefficient	GFE/RT
Oil	0.4	0.25	3.0	20,000	4.55
Gas	0.6	0.15	3.0	50,000	6.85
Aqueous	0.15	0.4	4.0	2000	2.63

petrophysical properties including pore size distribution, phase saturations, and wettability. The capillary pressure function is integrated with three-phase flash calculations to define the equilibrium state between oil, gas, and aqueous phase under reservoir conditions. The criterion for selection of cubic EOS roots originally proposed by Neshat et al. (2018) is extended for three-phase mixtures. This method minimizes the total Gibbs free energy of the mixture instead of minimizing the Gibbs free energy of each phase separately. The models are then used for simulation of primary production and solvent EOR processes in tight formations. Using rock and fluid properties for tight oil and gas reservoirs, the effect of water and condensate blockage as well as capillary pressure on production is simulated. The use of solvents to remove liquid blockage and to increase production rates is simulated for heterogeneous tight formations with high capillary pressure.

1.1. Three-phase flash with capillary pressure

At three-phase equilibrium condition, the chemical potential of each component *i* must be equal in all phases (Michelsen, 1994; Okuno et al., 2010). Equivalently, the fugacity of each component i in each phase must be equal. Component and overall mass balance must also be satisfied. In addition, with capillary pressure, there are two additional equations expressing capillary pressure equilibrium. For one mole of a three-phase mixture of oil, gas, and aqueous phases, the system of equations to be solved is as follows:

$$z_i = n_g x_{g,i} + n_o x_{o,i} + n_a x_{a,i} \tag{1}$$

$$\sum_{i=1}^{n} x_{g,i} = \sum_{i=1}^{n} x_{o,i} = \sum_{i=1}^{n} x_{a,i} = 1 \tag{2}$$

$$n_a + n_o + n_g = 1 \tag{3}$$

$$f_{o,g}(P_o, \vec{x}_o) = f_{g,i}(P_g, \vec{x}_g) = f_{a,i}(P_a, \vec{x}_a) \tag{4}$$

$$P_g - P_o = P_{c,og} \tag{5}$$

$$P_o - P_a = P_{c,oa} \tag{6}$$

The first three equations express overall and component mass balance. Equation (4) accounts for equality of the fugacity of each component *i* in all phases at the phase pressure. The PR EOS (Robinson and Peng, 1978) is used to calculate the fugacities. Equations (5) and (6) relate the phase pressures through capillary pressure terms between each two phase pair. Capillary pressure across an interface is a function of the surface curvature, wettability, and interfacial tension. The variation in pore size and interfacial curvature in porous media can be accounted for by saturation-dependent functions. The capillary pressures are calculated using a three-phase model proposed by Neshat and Pope (2017):

$$P_{c,og} = \sigma_{og} cos\theta_{og} \sqrt{\frac{\varphi}{k}} \left[\frac{b_o}{(S_o + S_a)^{a_o}} + \frac{b_g}{(S_g)^{a_g}} \right] \tag{7}$$

$$P_{c,oa} = \sigma_{oa} cos\theta_{oa} \sqrt{\frac{\varphi}{k}} \left[\frac{b_o}{(S_o)^{a_o}} + \frac{b_a}{(S_a)^{a_a}} \right] \tag{8}$$

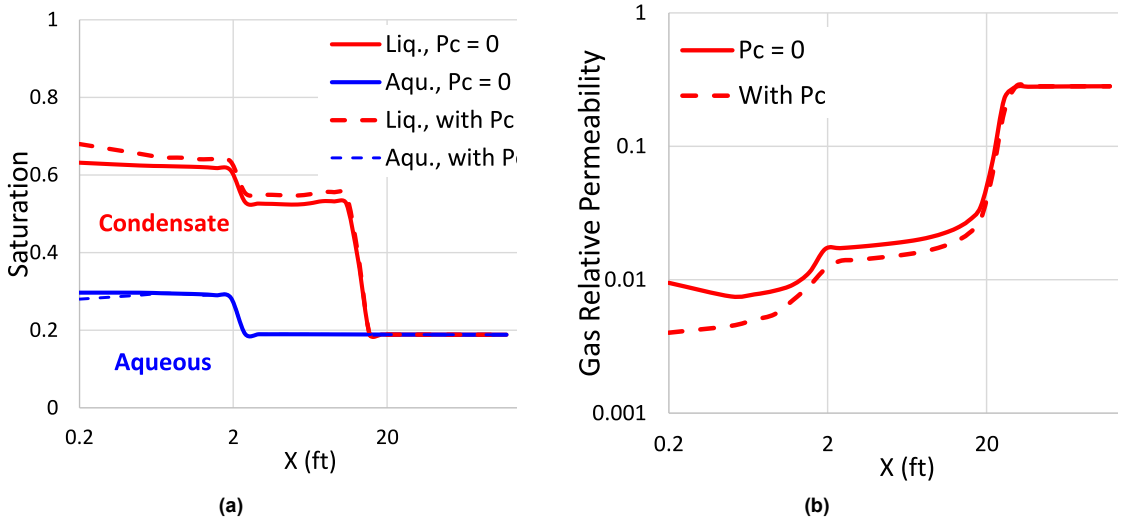

Fig. 4. Profiles of (a) aqueous and liquid saturations and (b) gas relative permeability within the matrix perpendicular to the fracture after 600 days of production from Eagle Ford gas-condensate reservoir. The x-axis is shown in log-scale to better indicate profile behavior near the fracture. Solid and dashed lines respectively show the simulations without and with the effect of capillary pressure.

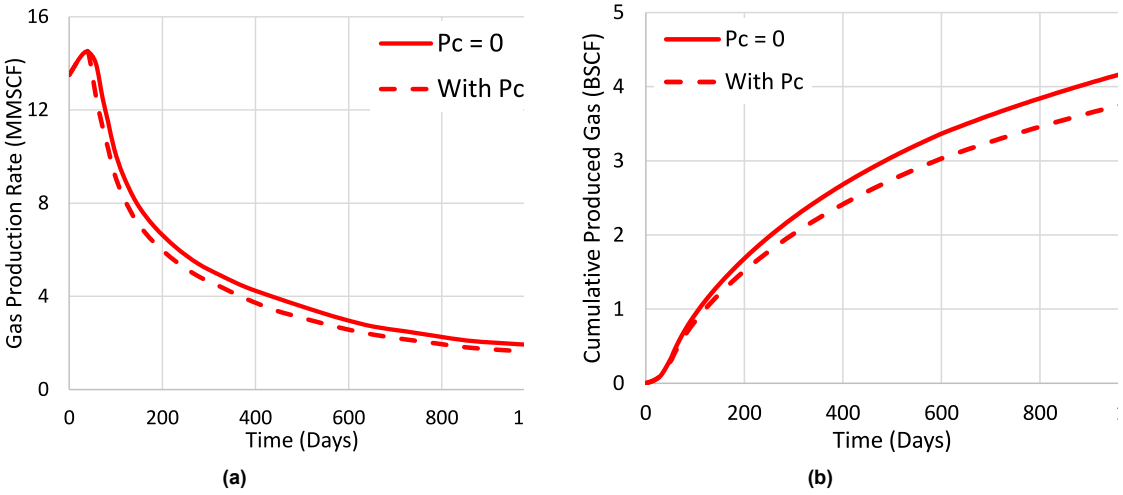

Fig. 5. Profiles (a) of gas production rate and (b) cumulative gas production from Eagle Ford gas-condensate reservoir during 1000 days of primary production. Solid and dashed lines respectively show the calculations without and with the effect of capillary pressure.

where the three saturations add to one in each equation and the fitting parameters (a_a, a_o, a_g, b_a, b_o, and b_g) are determined from experimental data. In the presence of a third phase, distribution of the fluids in different pore sizes can change depending on wettability. For example, water occupies the smallest pores of a water-wet rock and the hydrocarbon phases and the interface between them occupy the larger pores. This directly affects the capillary pressure between the phase pairs and is captured by Eqs. (7) and (8). For the applications discussed in this study, the gas phase is the non-wetting phase. The IFT between different phases is calculated using Macleod's equation with the exponent value suggested by Schechter and Guo (1988):

$$\sigma_{jk} = \left[\sum_{i=1}^{n_c} \chi_i \left(x_{j,i}\rho_j - x_{k,i}\rho_k\right)\right]^{3.88} \tag{9}$$

The procedure for solving three-phase flash with capillary pressure is described in the following section.

1.2. Algorithm for three-phase flash

Equations (1)–(6) were solved using the following successive substitution procedure:

1. Set $P_{c,og} = P_{c,oa} = 0$. Use the following equations to find an initial guess for equilibrium ratios, $K_{1,i} = \frac{x_{o,i}}{x_{g,i}}$ and $K_{2,i} = \frac{x_{o,i}}{x_{a,i}}$.

$$K_{1,i} = \frac{P_{r,i}}{\exp\left(5.37(1+\omega_i) \times \left(1 - \frac{1}{T_{r,i}}\right)\right)} \tag{10}$$

$$K_{2,i} = \frac{P_{r,i}}{10^6 \times T_{r,i}} \tag{11}$$

2. Solve the following coupled equations using Newton-Raphson method to find mole fractions, n_g, and n_a. n_o is determined by Eq. (3).

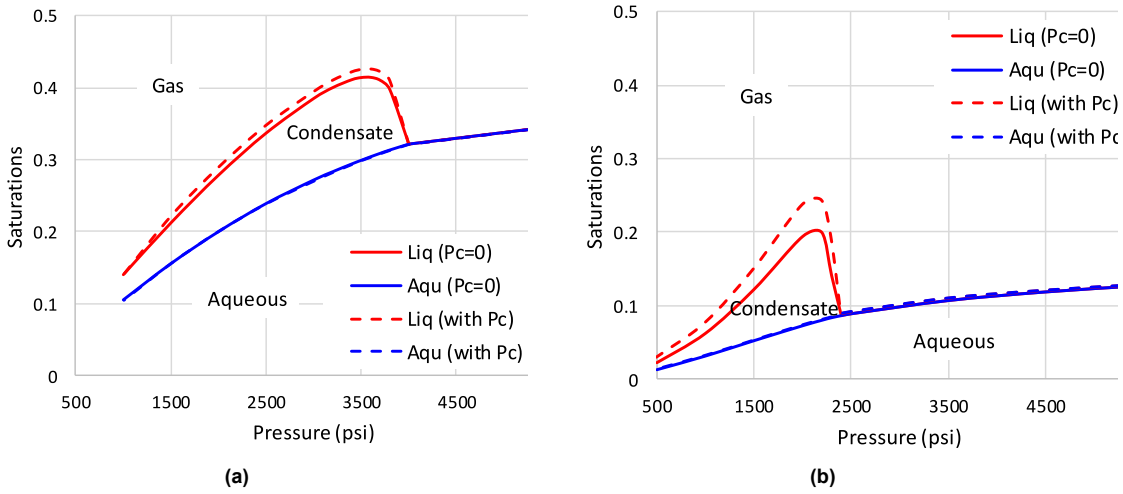

Fig. 6. Phase behavior of the mixture of (a) MeOH and (b) DME with Eagle Ford gas-condensate at 200 °F. The overall mole fraction of MeOH and DME is 0.25 in each case. Solid and dashed lines respectively show the calculations without and with the effect of capillary pressure on three-phase flash.

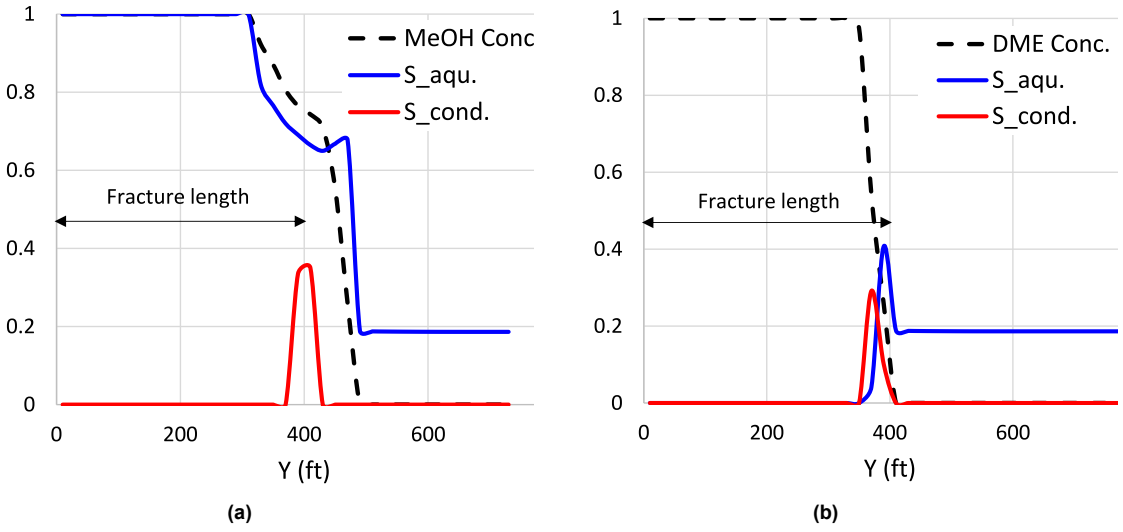

Fig. 7. Saturation profiles of aqueous and condensate phases within the matrix (a) MeOH is miscible with water (b) DME is miscible with both water and oil.

$$1=\sum_{i=1}^{n}\left[\frac{z_i(1-k_{1,i})}{n_g(1-k_{1,i})+n_a\left(\frac{k_{1,i}}{k_{2,i}}-k_{1,i}\right)-k_{1,i}}\right] \tag{12}$$

$$1=\sum_{i=1}^{n}\left[\frac{z_i k_{1,i}}{n_g(1-k_{1,i})+n_a\left(\frac{k_{1,i}}{k_{2,i}}-k_{1,i}\right)-k_{1,i}}\right] \tag{13}$$

3. Update $x_{o,i}$ using the following equation. Use the updated value along with the definition of $K_{1,i}$ and $K_{2,i}$ to update $x_{g,i}$, and $x_{a,i}$.

$$x_{g,i}=\frac{z_i}{\left(1+n_g\left(\frac{1}{k_{1,i}}-1\right)+n_a\left(\frac{1}{k_{2,i}}-1\right)\right)} \tag{14}$$

4. Solve the PR EOS to determine the compressibility factors, Z_o, Z_a, Z_g, for each phase. The procedure explained in Pedersen and Shaikh (2015) with van der Waals mixing rule can be followed with two modifications: First, the phase pressures are different (P_o, P_a, P_g). Second, EOS roots are selected in a way to minimize the total Gibbs free energy of the mixture.*
5. Calculate the fugacity coefficients, $\phi_{g,i}$, $\phi_{o,i}$, and $\phi_{a,i}$ at phase pressures.
6. Update $K_{1,i}$ and $K_{2,i}$.

$$k_{1,i}=\frac{\phi_{g,i}\,(P_o+P_{c,og})}{\phi_{o,i}\,P_o} \tag{15}$$

$$k_{2,i}=\frac{\phi_{a,i}\,(P_o+P_{c,oa})}{\phi_{o,i}\,P_o} \tag{16}$$

7. Calculate the iteration error ε, using the following equation.

$$\varepsilon=\max_i\left(ln\left(\frac{f_{o,i}}{f_{g,i}}\right),ln\left(\frac{f_{o,i}}{f_{a,i}}\right)\right) \tag{17}$$

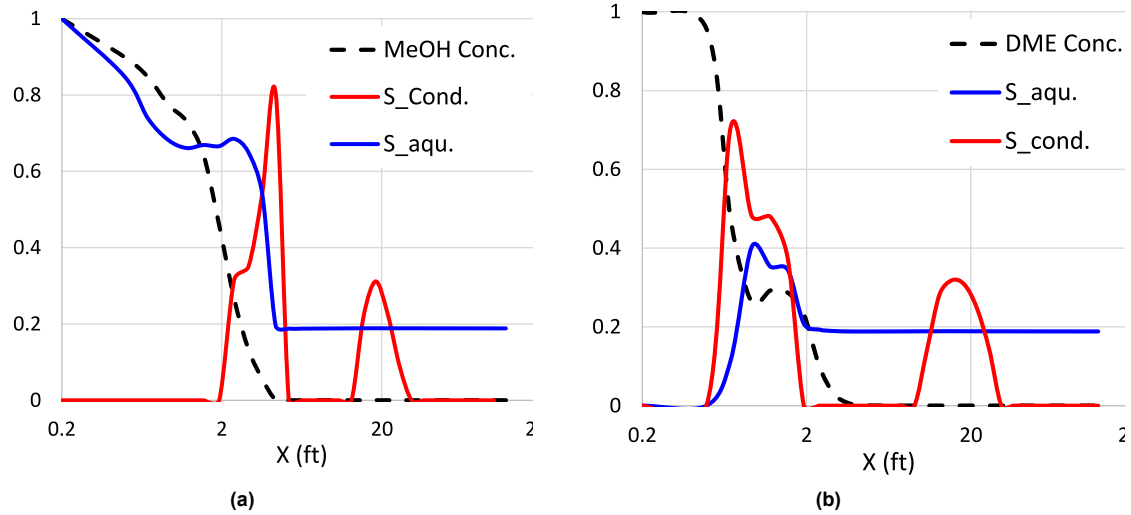

Fig. 8. Saturation profiles of aqueous and condensate phases within the matrix (a) MeOH is miscible with water and forms a continuous phase with formation water (b) DME is miscible with both water and oil and remains as a separate phase.

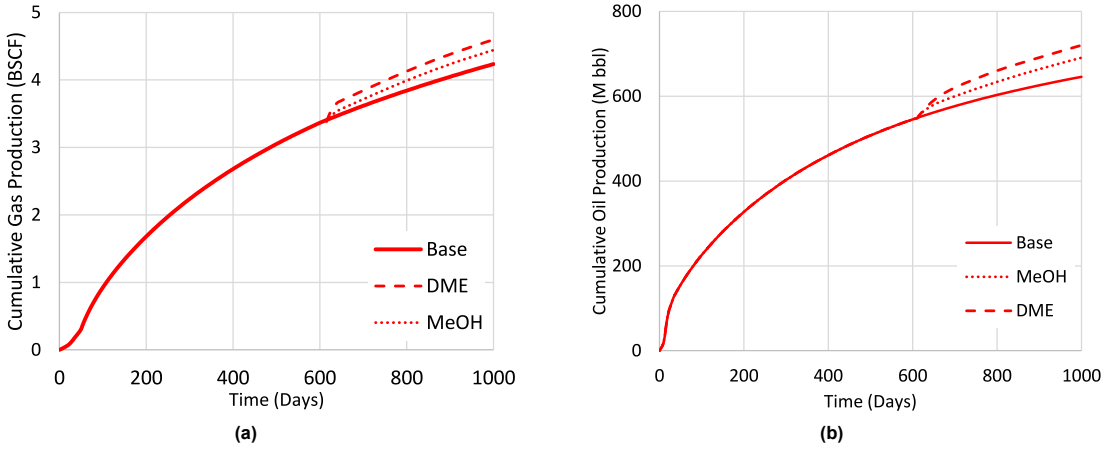

Fig. 9. Effect of solvent treatments on (a) cumulative gas and (b) cumulative oil (condensate) productions. All simulations include the effect of capillary pressure.

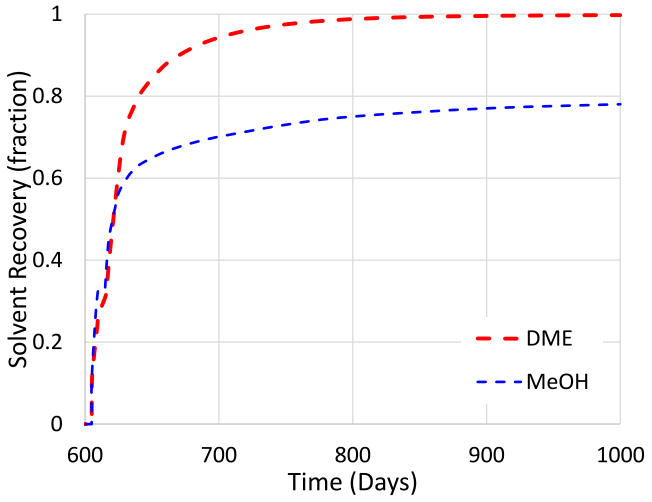

Fig. 10. Solvent recovery fraction after the stimulation.

Table 8
Reservoir properties (Middle Bakken).

Depth	13,000 ft
Reservoir thickness	300 ft
P (initial)	10,000 psi
Bubble point pressure	1950 psi
Oil density	0.69 gr/cm^3
Temperature	240 °F
Matrix Porosity	6%
Fracture porosity	30%
Fracture permeability	5 D
DME/MeOH Molecular diff. coef	0.03 ft^2/Day
Longitudinal dispersivity	25 ft
Tortuosity	100
S_w (initial)	22%
Production well BHP	2500 psi

Table 9
Relative permeability reference values (Middle Bakken). R and T are the universal gas constant and reservoir temperature, respectively.

	k_r^0	S_r	n	Trapping number coefficient	GFE/RT
Oil	0.5	0.20	3.0	15,000	3.65
Gas	0.45	0.25	3.0	40,000	6.35
Aqueous	0.2	0.4	3.5	3000	2.86

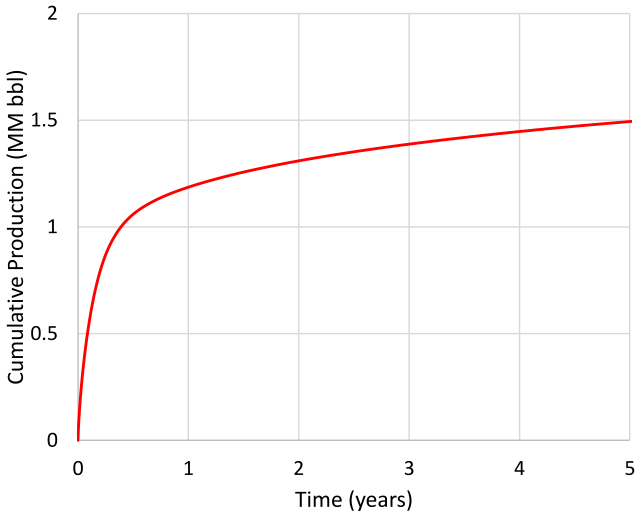

Fig. 11. Profile of primary production from Middle Bakken tight oil reservoir during 5 years of primary production.

8. Calculate $P_{c,og}$ and $P_{c,oa}$ using Eqs. (7) and (8) using updated values for IFT and saturations.
9. If $\varepsilon > 10^{-6}$, go to step 2. Otherwise, stop.

* The cubic EOS may have either one or three real roots. If there are three real roots, the middle root is discarded because it corresponds to an unconditionally unstable thermodynamic state. For the remaining two roots, the traditional method is to select the root that gives the lower Gibbs free energy (GFE) for the phase. Neshat et al. (2018) showed that this method does not always give a minimum in the total Gibbs free energy of the mixture. Therefore, a search was required to find the combination of EOS roots that gives the minimum total Gibbs free energy. When there are three real roots for a phase, combinations of the highest and lowest roots with roots for the other phases must be examined to determine the combination of roots with the lowest total Gibbs free energy corresponding to the thermodynamically correct solution. This approach is extended to three-phase equilibrium in this paper.

In compositional simulations, the flash algorithm explained above is performed for each gridblock at each time step using updated variables such as IFT, saturations and pressure. While successive substitution is relatively easy to implement numerically, it takes more iterations to converge as the non-linearity in the equations increases. For example, the capillary pressure functions expressed by Eqs. (7) and (8) become very steep at low wetting phase saturations which makes the system of equations more non-linear. One method to speed up the convergence at this condition is to solve Eqs. (1)–(5) simultaneously using an implicit formulation. The applications studied in this research were however limited to successive substitution.

1.3. Phase behavior of shale gas-condensate and tight oil mixtures

Coupled three-phase flash and capillary pressure models are used for modeling the phase behavior of reservoir fluids in unconventional formations. Fig. 1 shows the phase behavior of the Eagle Ford gas-condensate mixture using the three-phase model and also a two-phase model with fixed water saturation. The EOS (Orangi et al., 2011) and capillary pressure parameters used in these calculations are provided in Tables 1–3. Fig. 2 shows the same comparison between two- and three-phase flash models for phase behavior calculations of a Middle Bakken tight oil mixture. The EOS and capillary pressure parameters used for this case are provided in Table 3 through 5.

The saturation profiles of aqueous and total liquid (aqueous plus oil/condensate) phases in both cases clearly show the importance of using the three-phase model over the two-phase model. When pressure decreases, the concentration of water in the gas phase increases and thus, the aqueous saturation decreases. The lower water saturation can significantly change both oil-gas and oil-water capillary pressures. For example, it shifts the oil-gas interface into the smaller pores leading to higher oil-gas interface curvature and capillary pressure values. This can also be quantitatively investigated using Eqs. (7) and (8). Use of the three-phase models is necessary for accurate calculation of the capillary pressure and three-phase equilibrium with curved interfaces. The problem becomes more complex when solvents mix with reservoir fluids and change the phase behavior. All these effects can be accounted for

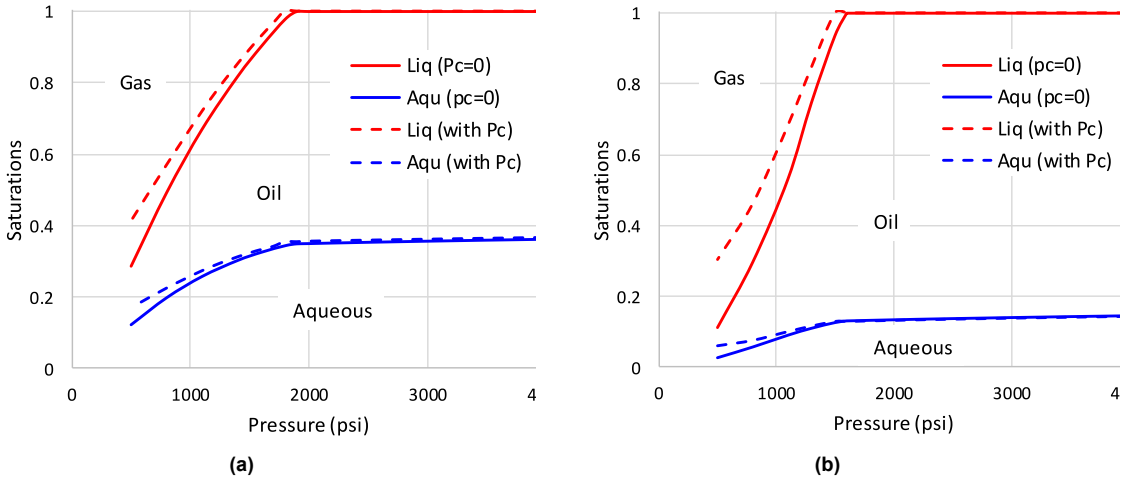

Fig. 12. Phase behavior of the mixture of (a) MeOH and (b) DME with Middle Bakken tight oil at 200 °F. The overall mole fraction of MeOH and DME is 0.25 in each case. Solid and dashed lines respectively show the calculations without and with the effect of capillary pressure on three-phase flash.

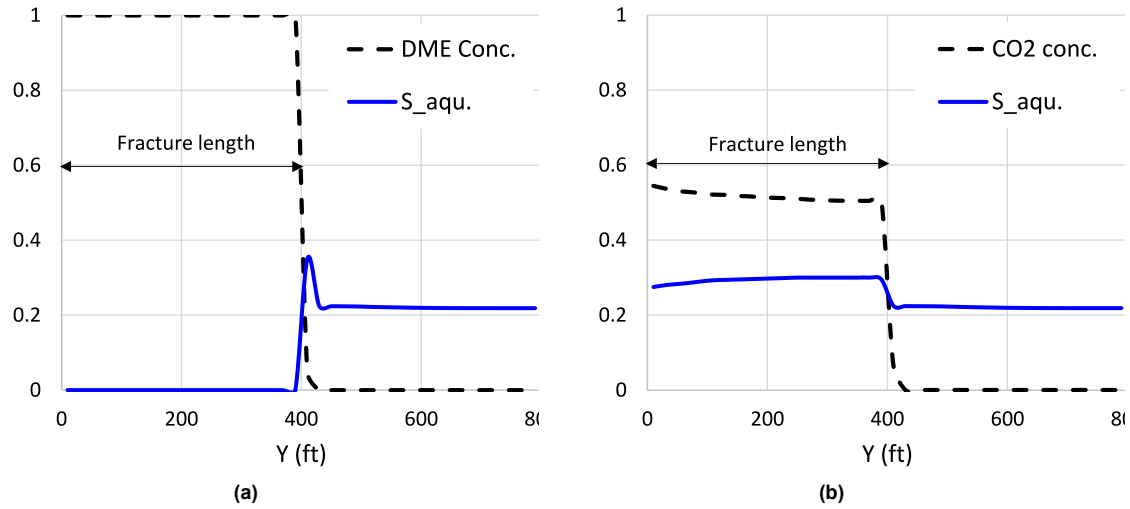

Fig. 13. Profiles of solvent concentration and aqueous saturations along the fracture length using (a) DME and (b) CO_2.

using the new coupled three-phase flash and capillary pressure models as will be discussed below.

1.4. Relative permeability model and compositional consistency

Relative permeability is a function of phase saturations, saturation history, and phase compositions. The compositional three-phase relative permeability model developed by Neshat and Pope (2017) is used in this study. The relative permeability is modeled using a Corey-type equation with all of the parameters dependent on composition:

$$k_{rj} = k_{rj}^{0}\left(\frac{S_j - S_{rj}}{1 - S_{rk} - S_{rl}}\right)^{n_j} \tag{18}$$

Capillary pressure and relative permeability are integrated petrophysical parameters and should follow consistent principles as explained below. To ensure compositional consistency in both capillary pressure and relative permeability models, the fitting parameters in Eqs. (7), (8) and (18) are interpolated by molar Gibbs free energies between reference values (Neshat and Pope, 2017). This alternative way to define the relative permeability and capillary parameters has three significant advantages over the traditional method of using phase labels. First, it ensures continuity in the calculated values of the relative permeability and capillary pressure as phases appear and disappear during compositional simulation. Second, relative permeability and capillary pressure parameters are evaluated independent of phase labels and are not affected by phase misidentification or flipping. Third, the GFE model can capture the effect of composition on relative permeability parameters consistent with experimental data (Jordan, 2016; Dria et al., 1993; Kalla et al., 2015).

The relative permeability parameters in Eq. (18) are also functions of trapping number (Pope et al., 2000) in this research. Trapping number quantifies the balance of viscous, gravitational and interfacial forces acting on a trapped phase. Mixing solvents with reservoir fluids can reduce the IFT between the phases drastically and increase the trapping number by a few orders of magnitude. Large variations in trapping number have a significant impact on relative permeability and must be considered for accurate simulation of such processes.

2. Case studies: solvent treatment of liquid blockage in tight reservoirs

The new three-phase flash coupled with the three-phase capillary pressure model has been implemented in the UTCOMP equation-of-state compositional simulator (Chang, 1990; Bang, 2007). This section

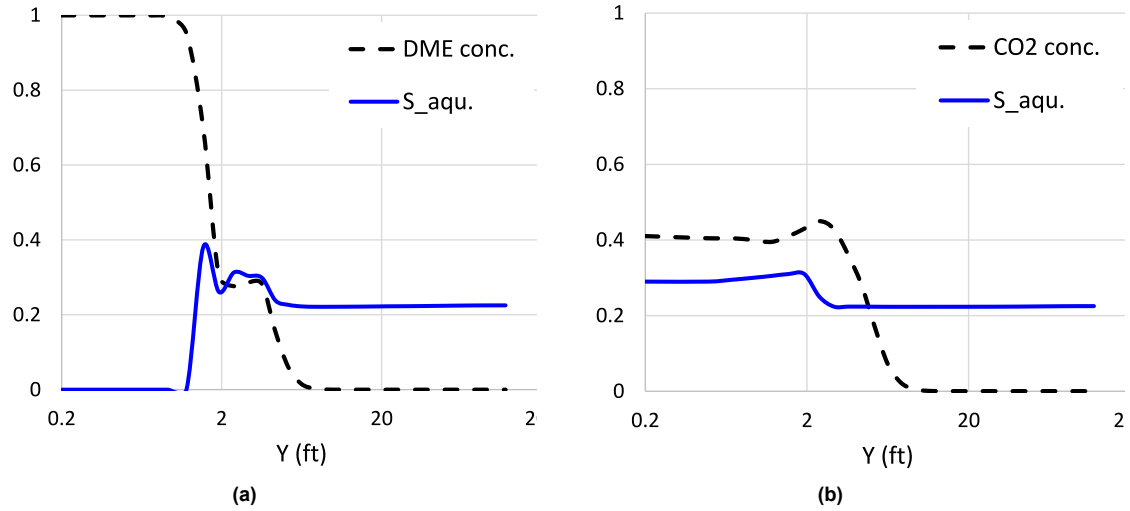

Fig. 14. Profiles of solvent concentration and aqueous saturations along the fracture length using (a) DME and (b) CO_2.

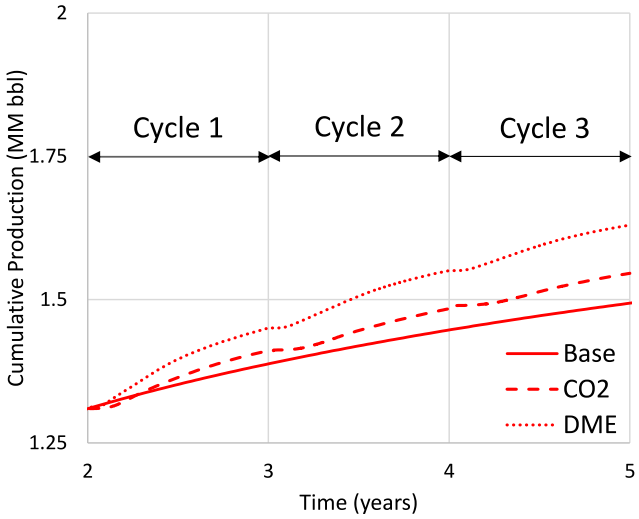

Fig. 15. Profiles of cumulative oil production from Middle Bakken tight oil reservoir during 3 cycles of solvent stimulation.

presents simulation of liquid and condensate blockage and solvent-based treatments in heterogeneous tight oil and gas reservoirs. Morel (1993) and Cronin et al. (2018) focused on diffusion-dominant flow in tight formations. The simulations presented here included diffusion and dispersion, but convection was dominant under the conditions of this study. Revil et al. (2013) reported tortuosity values in range of 100–200 for shale samples from the Middle Bakken reservoir. The lowest value ($\tau = 100$) was used to calculate the effective diffusion coefficient.

The well and hydraulic fractures configuration and computational domain used for simulation of both gas-condensate and tight oil simulation cases are illustrated in Fig. 3a. The length of the horizontal well is 12,500 ft and there are 50 hydraulic fractures along the well. The fracture aperture and permeability are 0.01 ft and 5D.

2.1. Eagle Ford shale gas-condensate reservoir

The Eagle Ford gas-condensate mixture described in the previous section was used for compositional simulations to investigate the effect of liquid blockage and its treatment on hydrocarbon production. The reservoir properties used for this simulation case are provided in Table 6. Fig. 3b shows a randomly generated permeability field. The average permeability, Dykstra-Parsons coefficient and anisotropy range are 1μD, 0.85 and 1800 ft, respectively. The grid is refined logarithmically near the fracture with the smallest cell size being 1 ft. Such refinement is necessary to capture the steep pressure change in the near fracture zone inside the matrix. The permeability field is generated after the refinement to provide a higher resolution in the region affected by fluid blockage and solvent treatment. Table 7 shows the relative permeability parameters and the corresponding Gibbs free energies (GFE) at reference conditions (Neshat and Pope, 2017). Fig. 4a shows the profiles of aqueous and liquid saturations within the matrix perpendicular to the fracture at point A (shown in Fig. 3b) after 600 days of primary production. The profile of liquid saturation in this figure shows the overall blockage caused by both aqueous and condensate phases that leads to a significant reduction in the gas relative permeability near the fracture as illustrated in Fig. 4b. This figure also shows that the capillary pressure increases the liquid saturation resulting in further reduction in gas relative permeability. Fig. 5a shows the gas production rate from the horizontal well during the first 1000 days of primary production. Once the production starts, a fraction of hydraulic fracturing fluid flows back and the production rate reaches to its maximum. After that, the production rate declines continuously as a result of condensate buildup near the hydraulic fractures. Fig. 5b shows the cumulative gas production. As shown in this figure, ignoring the effect of capillary pressure results in an error of about 10% in the cumulative produced gas.

Solvent-based huff-n-puff treatments are used to remove water and condensate blockage and increase gas production rate. The use of MeOH and DME is investigated in this example. Fig. 6 shows the phase behavior of a mixture of Eagle Ford gas-condensate hydrocarbon with the solvents at an overall mole fraction of 0.25. The EOS parameters used for these calculations are given in Tables 1, 2, 4 and 5 (Orangi et al., 2011). The EOS tuning parameters such as binary interaction coefficients (BICs) for MeOH and water (H_2O) were selected based on the experiments reported by Bang et al. (2010a). These authors showed that the PR EOS can model the phase behavior of MeOH, water and gas-condensate mixture very accurately if the EOS parameters are tuned properly. The DME properties were selected from Ganjdanesh et al. (2016). These authors tuned the BIC between DME and water to match experimentally measured phase behavior of the binary mixture of the two components reported in the literature (Pozo and Streett, 1974; Tallon and Fenton, 2010). Ratnakar et al. (2017) reported that the phase behavior of DME and brine mixtures depends on the brine salinity. In this research, we assume the salinity is constant and its effect is modeled by tuning the BICs. MeOH is miscible with water at all mole fractions while having small affinity for hydrocarbons as illustrated in Figs. 1a and 6a. Including MeOH to the mixture increases the saturation of the aqueous phase, but has only a small effect on condensate saturation and dew point pressure. MeOH also reduces the IFT between water and hydrocarbon phases which lowers the residual saturation values. Figs. 1a and 6b show that DME mixes with both aqueous and condensate phases and also reduces the dew point pressure significantly. DME can also reduce the IFT between water and hydrocarbon phases. This suggests that DME is a better solvent than MeOH because of its favorable phase behavior with reservoir fluids. The phase behavior profiles shown in Fig. 6 also show the significance of including 3-phase capillary pressure in calculations especially for hydrocarbon phases. For example, the saturation of condensate in the mixture of DME with reservoir fluids can be underestimated by more than 25% if capillary pressure is neglected.

After 600 days of production, solvent is injected through the hydraulic fractures for one day followed by 3 days of soak up time. Two separate scenarios of MeOH and DME injection were simulated. Fig. 7a shows the profile of MeOH concentration along the fracture after 1800 bbl per fracture injection and corresponding aqueous and liquid saturation profiles. MeOH has displaced aqueous and hydrocarbon phases from the fracture. Much of the displaced condensate has remained undissolved as a separate phase while the injected MeOH within the fracture has formed a continuous phase with the formation water. This is attributed to the miscibility of MeOH with water and its small affinity for hydrocarbons as shown earlier in Fig. 6a. One disadvantage of this behavior is partial flow back of condensate and aqueous phases when the well is put back on production. Fig. 7b shows the profile of DME concentration along the fracture after injection and corresponding aqueous and liquid saturation profiles. The injected DME volume is set to 1600 bbl per fracture to be consistent with the overall injection weight of MeOH. DME has also completely displaced the reservoir fluids from the hydraulic fracture. In this case, DME remains as a separate phase and dissolves much of the condensate and water. This helps to reduce the risk of flow back of the reservoir fluids in re-production stage. Fig. 8 shows the corresponding profiles of concentration and saturation for MeOH and DME injection cases inside the formation. Only first few feet close to the fracture is treated by the solvents since most of the blockage happens in this region. Chase gas such as methane or nitrogen could be used to drive the solvents deeper into the formation.

Fig. 9 shows the impact of solvent stimulation on cumulative gas and oil (condensate) production from the gas-condensate formation. The extra oil productions after one year of production following MeOH and DME treatments are about 6% and 9% respectively. Fig. 10 shows the

simulated recovery of the solvents. The recovered solvents can be recycled at the surfaceand used for another cycle. More than 95% of the DME has been recovered after 3 months of production whereas as less than 70% of the MeOH is recovered in the same time and about 20% remains in the residual water even after longer times.

2.2. Middle Bakken tight oil reservoir

This example investigates the use of CO_2, DME and MeOH as solvents to improve oil recovery from a heterogeneous tight oil reservoir. Fig. 2 shows the phase behavior used for simulation of a solvent huff-n-puff process. The reservoir and fluid properties are provided in Tables 8 and 9. The average permeability, Dykstra-Parsons coefficient and anisotropy range are 5 μD, 0.85 and 1500 ft, respectively. The bottom-hole pressure is higher than the bubble point pressure during primary production. Fig. 11 shows the cumulative oil production during the first 5 years of primary production. The rapid production decline illustrates the importance of solvent stimulation to improve the oil recovery.

Fig. 12 shows the phase behavior of mixtures of MeOH and DME with Middle Bakken tight oil reservoir fluids. Comparing Figs. 2a and 12a show that almost all of the MeOH mixes with the water and increases the aqueous saturation with little effect on the bubble point pressure of the hydrocarbons. Fig. 12a shows that at the same condition, DME mixes with both water and hydrocarbons, which lowers the aqueous saturation and the oil bubble point pressure. These results illustrate the significance of including capillary pressure in phase behavior calculations below the bubble point. For the mixture of DME with reservoir fluids at 1000 psi, the oil saturation can be underestimated by 30% if capillary pressure is ignored. Since the main purpose of solvent stimulation in this example is removal of water blockage, DME is preferred for injection into the tight oil reservoir. CO_2 is another solvent that is widely used for cyclic injection in tight oil reservoirs. CO_2 is less expensive than DME but it has very small solubility in water and cannot remove the water blockage.

Simulations were done to investigate the relative benefits of injecting different solvents following two years of primary production. The solvents are injected for one day followed by three days of soak time. Fig. 13a shows the DME concentration and aqueous saturation inside the fracture after the first injection cycle. DME has completely removed the water from the fracture. Fig. 13b shows the concentration of CO_2 and the aqueous saturation after the first CO_2 injection. The water has not been removed from the fracture because of the low solubility of CO_2 in water. Fig. 14 shows the profiles of solvent concentrations and aqueous saturation within the matrix after the stimulation. The injection process is repeated for three cycles. Fig. 15 shows the cumulative oil production after three cycles of solvent injection. About 10% more oil is produced following DME treatments compared to only 4% from CO_2 treatments. 89% of the DME is recovered and 87% of the CO_2 is recovered.

3. Summary and conclusions

The flash model was coupled with a three-phase capillary pressure model to include the effect of high capillarity on all three phases in tight formations. The significance of using the new coupled model was demonstrated by showing the phase behavior of the mixture of different water-soluble solvents with gas-condensate and tight oil reservoir fluids. The impact of water and condensate blockage on production from heterogeneous shale gas-condensate and tight oil reservoirs was studied. The use of methanol (MeOH), dimethyl ether (DME) and CO_2 in cyclic stimulation for liquid blockage removal was investigate.

Three-phase flash calculations are more realistic than two-phase calculations of the phase behavior. First, three-phase flash calculations account for the solubilities of water in hydrocarbons and solvents in the aqueous phase. Second, the impact of important petrophysical properties of tight formations such as pore size distribution and wettability are accounted for using the coupled three-phase capillary pressure model. Using the new phase behavior model in an equation-of-state compositional simulator significantly improves the accuracy of numerical simulations of recovery processes in high heterogeneous unconventional reservoirs. Simulation of primary production from Eagle Ford shale gas-condensate formation showed that water and condensate blockage within and around the hydraulic fractures reduces the hydrocarbon production substantially. Ignoring the effect of capillary pressure on phase behavior resulted in overestimating the production by about 10%. The use of both MeOH and DME for blockage removal was investigated. DME showed better performance because of its multicontact miscibility with oil. Rapid and high recovery of the injected DME under the simulated conditions show the advantage for using DME. Primary production and cyclic stimulation with CO_2 and DME in Middle Bakken tight oil formation was also studied. Because of very low solubility of CO_2 in water, CO_2 could not remove water blockage in the fracture or matrix. DME could completely clean the fracture and the neighboring region within the matrix resulting in a larger incremental oil recovery. The economics of the solvent stimulation processes can be optimized, for example, by using a chase gas in a multi-layered reservoir model, but it was beyond the scope of this study.

Declaration of competing interest

The authors declare that they have no known competing financial interests or personal relationships that could have appeared to influence the work reported in this paper.

Nomenclature

a_a	Capillary pressure exponent of aqueous
a_o	Capillary pressure exponent of oil
a_g	Capillary pressure exponent of gas
b_a	Capillary entry pressure of aqueous
b_o	Capillary entry pressure of oil
b_g	Capillary entry pressure of gas
k	Permeability
$K_{1,i}$	Equilibrium ratio between oil and gas
$K_{1,i}$	Equilibrium ratio between oil and aqueous
k_{rj}	Relative permeability of phase j
k^0_{rj}	Endpoint relative permeability of phase j
n_j	Relative permeability exponent of phase j
P_a	Aqueous pressure
P_o	Oil pressure
P_g	Gas pressure

$P_{c,og}$	Capillary pressure between oil and gas
$P_{c,oa}$	Capillary pressure between oil and aqeous
R	Gas constant
S_a	Aqeous saturations
S_o	Oil saturation
S_g	Gas saturation
S_{rj}	Residual saturation of phase j
u_L	Longitudinal advection velocity
$x_{a,i}$	Mole fraction of component i in aqueous
$x_{g,i}$	Mole fraction of component i in gas
$x_{o,a}$	Mole fraction of component i in oil
α_L	Longitudinal dispersion coefficient
ρ_j	Phase j molar density
σ_{jk}	interfacial tension between phases j and k
φ	Porosity
Θ_{og}	Contact angle for oil and gas
Θ_{oa}	Contact angle for oil and aqeous
$f_{a,i}$	Chemical potential of component i in aqueous
$f_{g,i}$	Chemical potential of component i in gas
$f_{o,i}$	Chemical potential of component i in oil
χ_i	Parachor of component i

Contribution

Sajjad Neshat: Development and implementation of the methods and algorithms, simulation cases; Ryosuke Okuno: Supervision; Gary Pope: Supervision

References

Al-Anazi, H.A., Walker, J.G., Pope, G.A., et al., 2005. A successful methanol treatment in a gas/condensate reservoir: field application. SPE Prod. Facil. 20 (1), 60–69. https://doi.org/10.2118/80901-PA. SPE-80901-PA.

Bang, V., 2007. Development of a Successful Chemical Treatment for Gas Well with Condensate or Water Blockage Damage. PhD dissertation. The University of Texas at Austin.

Bang, V., Pope, G.A., Sharma, M.M., 2010a. "Phase –behavior study of hydrocarbon/water/methanol mixtures ar reservoir conditions". SPE J. 15 (4), 952–962. https://doi.org/10.2118/102100-PA. SPE-102100-PA.

Bang, V., Pope, G.A., Sharma, M.M., Baran, J., Ahmadi, M., 2010b. A new solution to restore productivity of gas wells with condensate and water blocks. SPE Reservoir Eval. Eng. 13 (2), 323–331. https://doi.org/10.2118/116711-PA. SPE-102100-PA.

Bertoncello, A., Wallace, J., Blyton, C., Honarpour, M., Kabir, S., 2014. Imbibition and water blockage in unconventional reservoirs: well-management implications during flowback and early production. SPE Reservoir Eval. Eng. 17 (4), 497–506. https://doi.org/10.2118/167698-PA. SPE-167698-PA.

Brusilovsky, A.I., 1992. Mathematical simulation of phase behavior of natural multicomponent systems at high pressure with an equation of state. SPE Reservoir Eng. 7, 117–122. https://doi.org/10.2118/20180-PA.

Chang, Y., 1990. "Development and Application of an Equation of State Compositional Simulator. PhD dissertation. The University of Texas at Austin.

Cronin, M.B., Emami Meybodi, H., Johns, R.T., 2018. Diffusion-dominant proxy model for solvent huff-n-puff in ultra-tight oil reservoirs. In: Presented at the SPE Improved Oil Recovery Conference, Tulsa, OK, 14-18 April. SPE-190305-MS. https://doi.org/10.2118/190305-MS.

Dria, D., Pope, G., Sepehrnoori, K., 1993. Three-phase gas/oil/brine relative permeabilities measured under CO_2 flooding conditions. SPE Reservoir Eng. 8 (2), 143–150. https://doi.org/10.2118/20184-PA. SPE-20184-PA.

Ganjdanesh, R., Rezaveisi, R., Pope, G., Sepehrnoori, K., 2016. Treatment of condensate and water blocks in hydraulic-fractured shale-gas/condensate reservoirs. SPE J. 21 (2), 665–674. https://doi.org/10.2118/175145-PA. SPE-175145-PA.

Gupta, D.V.S., 2009. Unconventional fracturing fluids for tight gas reservoirs. In: Presented at the SPE Hydraulic Fracturing Technology Conference, Woodlands, Texas, 19-21 January. SPE-119424-MS. https://doi.org/10.2118/119424-MS.

Jiamin, J., Younis, R., 2016. Compositional simulation of enhanced hydrocarbons recovery for fractured shale gas-condensate reservoirs with the effects of capillary pressure and multi-component mechanisms. Nat Gas Sci & Eng 34 (1). https://doi.org/10.1016/j.jngse.2016.08.006, 262-1,275.

Jordan, P.B., 2016. Two-phase Relative Permeability Measurements in Berea Sandstone at Reservoir Conditions. Master's thesis. The University of Texas at Austin.

Kalla, S., Leonardi, S.A., Berry, D.W., Poore, L.D., Sahoo, H., Kudva, R., Braun, E.M., 2015. Factors that affect gas-condensate relative permeability. SPE J. 18 (1) https://doi.org/10.2118/173177-PA. SPE-173177-PA.

Michelsen, M.L., 1994. Calculation of multiphase equilibrium. Comput. Chem. Eng. 18 (7), 545–550. https://doi.org/10.1016/0098-1354(93)E0017-4.

Morel, D., Bourbiaux, B., Latil, M.,, 1993. Diffusion Effects in Gasflooded Light-Oil Fractured Reservoirs 1 (02), 100–109.

Nelson, P., 2009. Pore-throat sizes in sandstones, tight sandstones, and shales. AAPG 93 (3). https://doi.org/10.1306/10240808059.

Neshat, S.S., Okuno, R., Pope, G.A., 2018. A rigorous solution to the problem of phase behavior in unconventional formations with high capillary pressure. In: NA (Ed.), , 4th23. SPEJ.

Neshat, S.S., Pope, G.A., 2017. Compositional three-phase relative permeability and capillary pressure models using Gibbs free energy. In: Presented at the SPE Reservoir Simulation Conference, Montgomery, Texas, 20-22 February. SPE-182592-MS. https://doi.org/10.2118/182592-MS.

Nichita, D.V., 2018. Volume-based phase stability analysis including capillary pressure. Fluid Phase Equil. 492, 145–160. https://doi.org/10.1016/j.fluid.2019.03.025.

Nojabaei, B., Johns, R., 2013. Effect of capillary pressure on phase behavior in tight rocks and shales. SPE J. 16 (3) https://doi.org/10.2118/159258-PA.

Okuno, R., Johns, R.T., Sepehrnoori, K., 2010. A new algorithm for rachford-rice for multiphase compositional simulation. SPE J. 15 (2), 313–325. https://doi.org/10.2118/117752-PA.

Orangi, A., Nagarajan, N.R., Honarpour, M., Rosenzweig, 2011. Unconventional shale and gas-condensate reservoir production, impact of rock, fluid, and hydraulic fractures. In: Presented at SPE Hydraulic Fracturing Technology Conference, 24-26 January, Woodlands, TX. https://doi.org/10.2118/140536-MS.

Pedersen, Christensen, Shaikh, J., 2015. In: NA (Ed.), Phase behavior of petroleum reservoir fluids. CRC Press.

Pope, G., Wu, W., Narayanaswamy, G., Delshad, M., Sharma, M.M., Wang, P., 2000. Modelling relative permeability effects in gas-condensate reservoirs with a new trapping model. J Res Eval & Eng 3 (2). https://doi.org/10.2118/62497-PA. SPE-62497-PA.

Pozo, M.E., Streett, W.B., 1974. Fluid phase equilibria for the system dimethyl ether/water from 50 to 220.degree.C and pressures to 50.9 MPa. Chem. & Eng. Data. 29 (3), 324–329. https://doi.org/10.1021/je00037a030.

Ratnakar, R.R., Dindoruk, B., Wilson, L., 2017. Phase behavior experiments and PVT modeling of DME-brine-crude oil mixtures based on Huron-Vidal mixing rules for EOR applications. Fluid Phase Equil. 24, 49–62. https://doi.org/10.1016/j.fluid.2016.11.021.

Revil, A., Woodruff, W.F., Torres-Verdin, C., Prasad, M., 2013. Complex conductivity tensor of anisotropic hydrocarbon-bearing shales and mudrocks. Geophysics 78 (6). https://doi.org/10.1190/geo2013-0100.1.

Robinson, D.B., Peng, D.Y., 1978. The Characterization of the Heptane and Heavier Fractions for GPA Peng-Robinson Programs. *Gass Processors Association*. RR-28.

Sanaei, A., Jamili, A., Callard, J., 2014. In: Effect of Pore Size Distribution and Connectivity on Phase Behavior and Gas Condensate Production from Unconventional Resources," Presented at the SPE Unconventional Resources Conference, 1-3 April, Woodlands, TX. https://doi.org/10.2118/168970-MS. SPE-168970-MS.

Sandoval, D.R., Michelsen, M.L., Yan, W., Stenby, E.H., 2019. VT-based phase envelope and flash calculations in the presence of capillary pressure. Ind. Eng. Chem. Res. (58), 5291–5300. https://doi.org/10.1021/acs.iecr.8b05976.

Sayed, M.A., Al-Muntasheri, G.A., 2016. Mitigation of the effect of condensate banking: a critical review. SPE Prod. Oper. 31 (2), 85–102. https://doi.org/10.2118/168153-PA. SPE-168153-PA.

Schechter, D.S., Guo, B., 1988. Parachors based on modern physics and their uses in IFT prediction of reservoir fluids. SPE J. 1 (3), 207–217. https://doi.org/10.2118/30785-PA.

Sherafati, M., Jessen, Christian, 2017. Stability analysis for multi-component mixtures including capillary pressure. Fluid Phase Equil. 433, 56–66. https://doi.org/10.1016/j.fluid.2016.11.013.

Siripatrachai, N., Ertekin, T., Johns, R., 2017. Compositional simulation of hydraulic fractured tight formation considering the effect of capillary pressure on phase behavior. SPE J. 22 (4) https://doi.org/10.2118/179660-PA, 1,046-1,064. SPE-149660-PA.

Tallon, S., Fenton, K., 2010. The solubility of water in mixture of dimethyl ether and carbon dioxide. Fluid Phase Equil. 298 (1), 60–66. https://doi.org/10.1016/j.fluid.2010.07.009.